Removal of the High-Potential [4Fe–4S] Center of the β-Subunit from *Escherichia coli* Nitrate Reductase. Physiological, Biochemical, and EPR Characterization of Site-Directed Mutated Enzymes†

Valérie Augier,‡ Marcel Asso,§ Bruno Guigliarelli,§ Claude More,§ Patrick Bertrand,§ Claire-Lise Santini,‡ Francis Blasco,‡ Marc Chippaux,‡ and Gérard Giordano*,‡

Laboratoire de Chimie Bactérienne, CNRS, 31, chemin Joseph Aiguier, 13402 Marseille Cedex 9, France, and Laboratoire d'Electronique des Milieux Condensés, URA CNRS 784, Université de Provence, Marseille, France

Received December 23, 1992; Revised Manuscript Received March 1, 1993

ABSTRACT: The β-subunit of the nitrate reductase of *Escherichia coli* contains four groups of Cys residues (I–IV) which are thought to bind the single [3Fe–4S] center and the three [4Fe–4S] centers. The first or second Cys residue of group I was substituted by site-directed mutagenesis with Ala or Ser. Physiological, biochemical, and EPR studies were performed on the mutated enzymes. With small variations, the properties of these mutant enzymes do not differ from one another. They were found to be as abundant and as stably bound to the membrane as the native enzyme, provided the γ-subunit was present. Although physiological activity was reduced, it was sufficient to allow growth on nitrate. The study of variations in EPR intensity as a function of the redox potential indicated that these enzymes only contained three iron–sulfur centers instead of the usual four in the native enzyme. Spectral EPR analysis showed that the [4Fe–4S] center of high redox potential (center 1, +80 mV) was missing. The loss of this center did not affect the stable integration of the other three centers. The data presented here are in total contrast to those we have reported for each of the other three centers (centers 2–4), the loss of which was detrimental to the integration of all centers and to the integration of the molybdenum cofactor (Augier et al., in press). Taken together, our results demonstrated that the first and second Cys residues of group I are the ligands of the [4Fe–4S] center (center 1, +80 mV) and that this center participates in electron transfer, but is dispensable. On the basis of these results, it is proposed that the [3Fe–4S] center (center 2, +60 mV) also plays a biological role and that in the native enzyme both high-potential centers, centers 1 and 2, contribute independently and in parallel to the electron transfer to the molybdenum cofactor.

Nitrate reductase allows *Escherichia coli* to use nitrate as a terminal electron acceptor during anaerobic growth. It is a membrane-bound complex of three subunits, α, β, and γ (MacGregor, 1975; Graham & Boxer, 1980). The current scheme proposed for electron transfer is as follows: the γ-subunit, a *b*-type cytochrome, receives electrons from quinones in the membrane and transfers them to iron–sulfur centers of the β-subunit. This subunit, in turn, delivers them to the molybdenum cofactor carried by the α-subunit, where reduction of nitrate to nitrite occurs. Although previous spectroscopic studies have shown the presence of [3Fe–4S] and [4Fe–4S] clusters in nitrate reductase (Johnson et al., 1985), the stoichiometry and the redox properties of these centers have been determined recently. We have demonstrated (Guigliarelli et al., 1992) that the enzyme contains one [3Fe–4S] and three [4Fe–4S] centers, which fall into two classes according to their redox potentials: one of the [4Fe–4S] centers, center 1 (+80 mV), and the [3Fe–4S] center, center 2 (+60 mV), have relatively high redox potentials, while the remaining two [4Fe–4S] centers have markedly negative potentials (–200 mV for center 3 and –400 mV for center 4). Their full reduction leads to a broad, structureless EPR[1] spectrum typical of iron–sulfur centers coupled by magnetic interactions. These centers are likely to be carried by the single β-subunit which, according to the *narGHJI* operon sequence (Sodergren & DeMoss, 1988; Blasco et al., 1989), has four cysteinyl arrangements (groups I–IV) of the type which form iron–sulfur centers in ferredoxins.

The role of iron–sulfur centers in electron transfer and the identification of the amino acid residues which act as ligands have been reported for several proteins. In these studies, site-directed mutagenesis was used to alter certain Cys residues and to show that they are ligands of the iron–sulfur centers (Kent et al., 1989; Werth et al., 1990; May et al., 1991; Rothery & Weiner, 1991; Manodori et al., 1992). In a previous work (Augier et al., in press), we have shown that conversion of the first Cys residue of groups II–IV to alanine results, in all cases, in a β*-subunit which has lost all four iron–sulfur centers and not just a single one, as would have been expected. It was concluded that the three iron–sulfur centers coordinated by these Cys residues are in such structural interdependency that the loss of any one of the centers would be detrimental to the integration and/or stabilization of all other centers in the enzyme. In that work, however, none of the Cys residues of group I was substituted. It was therefore of interest to determine whether the center coordinated by these group I Cys residues could be lost without leading to the lack of all centers.

In this article, we report on the substitution of the first and second Cys residues of group I of the enzyme. The center coordinated by these Cys residues has been unambiguously identified as the high-potential [4Fe–4S] center (center 1, +80 mV), and it is shown that its loss results in a mutant

† This research was supported, in part, by the ARC and by the Interface Chimie Biologie.

* Author to whom correspondence should be addressed. Telephone: (33) 91.16.44.31. Fax: (33) 91.71.89.14.

‡ Laboratoire de Chimie Bactérienne.

§ Université de Provence.

[1] Abbreviations: IPTG, isopropyl β-D-thiogalactopyranoside; EPR, electron paramagnetic resonance; NR, nitrate reductase.

0006-2960/93/0432-5099$04.00/0

Table I: Bacterial Strains and Plasmids

strain or plasmid	description/genotype[a]	source
E. coli strains		
MC4100	*ara*D139D(*lac*IPOZYA–*arg*F)*rps*L,*thi*	Casadaban (1976)
LCB 79	MC4100 with ϕ79 (*nar–lac*)	Pascal (1982)
plasmids		
pVA7	pACYC184Cm^R(*narJ*)$^+$	Augier (in press)
pVA14	pACYC184Cm^{R}Tet^R-(*narJI*)$^+$	Augier (in press)
pVA 50	pJF119EHAp^R(*narGH*)$^+$	Augier (in press)
pVA 50-C_{16}A	pJF119EHAp^R(*narGH*-[C16→A16])$^+$	this study
pVA 50-C_{19}A	pJF119EHAp^R(*narGH*-[C19→A19])$^+$	this study
pVA 50-C_{19}S	pJF119EHAp^R(*narGH*-[C19→S19])$^+$	this study

[a] Ap^R, ampicillin-resistant; Cm^R, chloramphenicol-resistant; Tet^R, tetracycline-resistant.

enzyme with reduced activity but which possesses the three other centers with unchanged characteristics.

EXPERIMENTAL PROCEDURES

Bacterial Strains and Plasmids. All *Escherichia coli* strains and plasmids used in this study are listed in Table I. Plasmid pVA50 (11.3 kb) carries the *narG* and *narH* genes under the *tac* promoter (*Ptac*). Plasmid pVA7 (5.3 kb) carries the *narJ* gene under the nitrate reductase promoter (*Pnar*). Plasmid pVA14 (6.4 kb) carries the *narJ* and *narI* genes under the nitrate reductase promoter (*Pnar*). All of these plasmids have been described previously by Augier et al. (in press).

Oligonucleotide-Directed Mutagenesis and Expression of the Altered narH Gene. Oligonucleotide-directed mutagenesis was performed using the Amersham in vitro mutagenesis kit on the basis of the method of Taylor et al. (1985), as described previously by Augier et al. (in press).

Expression of nitrate reductase complexes can be obtained from separate transcriptional units (Blasco et al., 1992). For reasons detailed in the previous article (Augier et al., in press), pVA50 has been used with pVA7 to express concomitantly the α-, β-, and δ-polypeptides of the nitrate reductase (i.e., without cytochrome *b*) or with pVA14 to express the complete nitrate reductase (α-, β-, δ-, and γ-polypeptides).

Manipulation of DNA. Recombinant DNA techniques, i.e., isolation of plasmid DNA, restriction enzyme digestion, polymerase polishing, ligation, transformation, and electrophoresis, were essentially adapted from Maniatis et al. (1982). Unless otherwise indicated, the enzymes were purchased from BRL and used with the supplied or recommended buffer.

Culture Conditions. Strains were grown on basal medium as described previously (Giordano et al., 1978). For the induction of nitrate reductase, potassium nitrate was added to a final concentration of 1 g L^{-1}.

For anaerobic growth on minimal medium, Difco yeast extract and Difco Bactopeptone were omitted, glucose was replaced by glycerol (2 g L^{-1}), and amino acids required by the strains (all at 10 mg L^{-1}) were added to the medium.

Strains carrying plasmids were grown by adding the appropriate antibiotics (ampicillin, 50 μg mL^{-1}; chloramphenicol, 10 μg mL^{-1}) and, when needed, IPTG (0.2 mM) to induce the *tac* promoter (*Ptac*).

Preparation of Subcellular Fractions. The cells were harvested during the exponential phase of growth, suspended in 50 mM Tris-HCl (pH 7.6), and disrupted in a French press. The soluble and membrane fractions were obtained as described by Saracino et al. (1986). All procedures were performed at 4 °C.

Enzyme Assays. Nitrate reductase activity was measured spectrophotometrically (Jones & Garland, 1977) by the oxidation of reduced benzyl viologen, which leads to the reduction of nitrate to nitrite. One unit of nitrate reductase activity is the amount catalyzing the production of 1 μmol of nitrite min^{-1} (mg of protein)$^{-1}$. Proteins were estimated by the technique of Lowry et al. (1951).

Formate-dependent nitrate reduction was measured on whole cells with formate as the electron donor (Pichinoty, 1969). The nitrite formed was measured as described by Iobbi et al. (1987).

Quantification of Nitrate Reductase. Quantification of the nitrate reductase antigen present in nitrate reductase preparations was performed by rocket immunoelectrophoresis analysis (Graham et al., 1980). The reference curves were established with fully purified nitrate reductase A and immunoadsorbed anti-nitrate reductase A serum. The samples (6 μL) were electrophoresed at 2 mA overnight on 4 × 4 cm (1% w/v) agarose plates buffered with 20 mM sodium barbital (pH 8.6) containing (1% w/v) Triton X-100 and 0.05% (w/v) sodium azide. Antiserum (100 μL) was included in the agarose medium.

Limited Proteolysis by Trypsin. Partially purified wild-type or mutated nitrate reductases (50 μg of protein) were incubated with an equal mass of trypsin for 1 h at 37 °C at pH 7.6. Trypsin was inactivated by the addition of disaggregation buffer followed by a heat treatment, and the samples were loaded on SDS–PAGE (7.5% w/v).

Polyacrylamide Gels. Electrophoresis under denaturing conditions was carried out on polyacrylamide gels (7.5% w/v) at pH 8.8. Polyacrylamide gel electrophoresis in the presence of SDS was performed as described by Laemmli (1970).

Western Blotting Analysis. After electrophoresis by SDS–PAGE (7.5%), the proteins were electrotransferred to a sheet of nitrocellulose in buffer containing 20% methanol, as described previously by Towbin et al. (1979). In all of our experiments, the molecular weights of the native and mutant nitrate reductases were estimated with standards stained by the nonpermanent stain Ponceau S before incubation with antibodies.

Partial Purification of Mutant Nitrate Reductases. Partial purification of mutant nitrate reductases was performed as previously described by Augier et al. (in press).

Redox Titration and EPR Spectroscopy. The redox titration and EPR experiments were performed on control and mutant nitrate reductases as previously described by Guigliarelli et al. (1992).

RESULTS

Construction of Mutant Nitrate Reductases by Site-Directed Mutagenesis of the NarH Subunit. Cys_{16} and Cys_{19}, the first two cysteinyl residues in group I of the NarH subunit, are likely to be involved in liganding an iron–sulfur center. They were individually changed by site-directed mutagenesis to Ala (Cys_{16}) and to Ala or Ser (Cys_{19}). The mutated DNA fragments of interest were totally sequenced to check the presence of the specified mutation and to ensure that no other mutation had been introduced. This led to mutant subunits designated $\beta(C_{16}A)$, $\beta(C_{19}A)$, and $\beta(C_{19}S)$.

In all of this work, the control and mutated enzymes were overproduced from plasmids in strain LCB79 devoid of the chromosomal *narGHJI* genes. Plasmid pVA50 (carrying *narGH* genes) was used together with either plasmid pVA14

Table II: Benzyl Viologen Activity, Formate–Nitrate Reductase Activity, and Anaerobic Growth on Glycerol–Nitrate Medium of Strains Transformed with pVA14 and Various pVA50 Plasmids[a] Carrying the Mutated *narH* Gene

strain	benzyl viologen nitrate reductase activity in crude extracts: total activity[b]	specific activity[c]	%	formate–nitrate reductase activity: nmol of nitrite formed[d] (min^{-1} mg^{-1} dry weight)	%	growth on glycerol–nitrate medium (double time in min)
MC 4100	72	57	95	59	103	190
LCB79	1	<0.3	<1	<0.3	<1	no growth
LCB79/pVA14+pVA50	590	60	100	57	100	180
LCB79/pVA14+pVA50C_{16}A	97.5	4.8	8	19.5	34	300
LCB79/pVA14+pVA50C_{19}A	71.5	5.5	9	19	33	320
LCB79/pVA14+pVA50C_{19}S	72	7.2	12	17	30	280

[a] Plasmid pVA14 encodes for the *narJ* and *narI* genes. pVA50 encodes for the *narG* and *narH* genes (Figure 1). [b] Total benzyl viologen nitrate reductase activities of crude extracts were expressed in μmol of nitrate reduced min^{-1}. [c] Specific benzyl viologen nitrate reductase activities were expressed in μmol of nitrate reduced min^{-1} (mg of nitrate reductase)$^{-1}$ and as a percent of the specific activity found in strain LCB79/pVA14+pVA50. [d] Formate–nitrate reductase activities, from cells grown anaerobically in the presence of glucose (2 g L^{-1}), were measured as described in the Experimental Procedures. Activity is given as nmol of nitrite formed min^{-1} mg^{-1} dry weight and as a percent of the activity found in strain LCB79/pVA14+pVA50.

(*narJ*$^+$*I*$^+$), to express a physiologically active nitrate reductase $\alpha\beta\gamma$, or with plasmid pVA7 (*narJ*$^+$), to express a soluble, benzyl viologen active nitrate reductase $\alpha\beta$ (Table I). In this last case, as previously demonstrated (Augier et al., in press), the γ-subunit is eliminated and its EPR signals can no longer interfere with those of the iron–sulfur centers of the enzyme.

Properties of the Mutant Nitrate Reductases in Cells Containing α-, β-, δ-, and γ-Polypeptides. Crude extracts of cells expressing all *nar* genes carried by plasmids and grown anaerobically in the presence of nitrate display a total benzyl viologen nitrate reductase activity that is about 8 times that of the parental strain MC4100 expressing the *narGHJI* chromosomal copy (Table II). The effects of the substitutions introduced in the first cysteine group of NarH are shown in Table II. Extracts containing $\beta(C_{16}A)$, $\beta(C_{19}A)$, or $\beta(C_{19}S)$ mutant subunits have a reduced but significant benzyl viologen-dependent nitrate reductase activity which is 8–12% of the specific activity of control cell extracts.

Quinones are the physiological electron donors to the membrane-bound nitrate reductase for the reduction of nitrate. They are reduced during the oxidation of formate by formate dehydrogenase and provide electrons to the γ-subunit of the nitrate reductase, which is believed to transfer them to the α-subunit via the iron–sulfur centers of the β-subunit. Table II shows that cells expressing the *narH*(C_{16}A), *narH*(C_{19}A), or *narH*(C_{19}S) mutated genes have a physiological formate-dependent nitrate reductase activity which is 30–34% of the activity in control cells.

Cells expressing the mutated enzymes were then grown under anaerobic conditions in nitrate minimal medium supplemented with glycerol. Under these conditions, only those cells capable of performing a functional electron transfer from quinones to nitrate can grow. As reported in Table II, all three mutants are capable of growth, although they grow more slowly than the control cells. Doubling times were 280–300 min for the mutants compared with 180 min for the control cells. The results of these growth experiments correlated well with the formate-dependent nitrate reductase activities observed for the different mutant strains and indicated that, although slowed down, the electron transfer actually takes place in the mutated enzyme.

Physiological electron transfer from quinones in the membrane to nitrate in the cytoplasm can only occur when the nitrate reductase is membrane-bound. Table III indicates that 50–74% of the total benzyl viologen-dependent activity of the cells expressing the *narH*(C_{16}A), *narH*(C_{19}A), or *narH*(C_{19}S) alleles is found in the membrane fraction; this

Table III: Nitrate Reductase Activities and Amounts of Immunoprecipitated Nitrate Reductase in Soluble and Membrane Fractions of Strains Transformed with pVA14 and Various pVA50 Plasmids Carrying the Mutated *narH* Gene

strain		benzyl viologen nitrate reductase activity: total activity[a]	%	specific activity[b]	immunoprecipitated nitrate reductase: mg of protein[a]	%
MC4100	M	46	69	57	0.8	70
	S	20.5	31	60	0.34	30
LCB79/ pVA14+ pVA50	M	396	67	61	6.5	66
	S	197	33	58	3.4	34
LCB79/ pVA14+ pVA50C_{16}A	M	47	50	6.5	7	52
	S	47	50	7	6.5	48
LCB79/ pVA14+ pVA50C_{19}A	M	34.5	74	4.5	8	73
	S	12	26	4	3	27
LCB79/ pVA14+ pVA50C_{19}S	M	48.5	56	8	6.1	60
	S	38	44	9.5	4	40

[a] Total benzyl viologen nitrate reductase activities of membrane (M) and soluble (S) fractions were expressed in μmol of nitrate reduced min^{-1} or in % of the sum of the activities present in the soluble and membrane fractions. [b] Specific benzyl viologen nitrate reductase activities were expressed in μmol of nitrate reduced min^{-1} (mg of nitrate reductase)$^{-1}$. [c] The amount of total immunoprecipitated nitrate reductase in membrane and soluble fractions was expressed in mg of enzyme per 100 mg of protein, estimated by rocket immunoelectrophoresis as described in the Experimental Procedures, and in % of the sum of the immunoprecipitated nitrate reductase present in the soluble and membrane fractions.

confirms the prediction that the mutations had not greatly interfered with the enzyme's ability to bind to the membrane.

In order to better appreciate the effect of the mutations on the enzymatic activity, the technique of rocket immunoelectrophoresis was used to quantify the amounts of mutant and wild-type enzymes present in the soluble and membrane fractions, as well as to determine the specific activity of each mutant or wild-type nitrate reductase. Table III shows, firstly, that enzyme levels in the mutant and wild-type strains are the same when measured by the immunoprecipitation technique: 10.1–13.5 mg of protein was detected for the mutants compared with 9.9 mg for the control. Secondly, the partition of the enzyme between soluble and membrane fractions is in good agreement with the partition of the benzyl viologen-dependent activity. Taken together, these observations suggest that the mutations do not play any essential role at the level of enzyme stability and subcellular partition, but that electron transfer through these enzymes is affected.

Table IV: Nitrate Reductase Activities and Amounts of Immunoprecipitated Nitrate Reductase in the Soluble Fraction of Strains Transformed with pVA7 (Lacking *narI* Gene) and Various pVA50 Plasmids Carrying the Mutated *narH* Gene

	benzyl viologen nitrate reductase activity in soluble fraction			immunoprecipitated nitrate reductase in soluble fraction	
strain	total activity[a]	specific activity[b]	%	mg of protein[c]	%
LCB79/pVA7+pVA50	590	56	100	10.5	96
LCB79/pVA7+pVA50C_{16}A	63	5	9	12.5	98
LCB79/pVA7+pVA50C_{19}A	71.5	5.5	10	13	97
LCB79/pVA7+pVA50C_{19}S	58	8	14	7	95

[a] Total benzyl viologen nitrate reductase activities of the soluble fraction were expressed in μmol of nitrate reduced min^{-1}. [b] Specific benzyl viologen nitrate reductase activities were expressed in μmol of nitrate reduced min^{-1} (mg of nitrate reductase)$^{-1}$ and in % of the specific activity found in strain LCB79/pVA7+pVA50. [c] The amount of immunoprecipitated nitrate reductase in the soluble fraction of each strain was expressed in mg of enzyme per 100 mg of protein, estimated by rocket immunoelectrophoresis, and in % of the immunoprecipitated nitrate reductase present in the corresponding crude extract.

Properties of the Mutant Nitrate Reductases in Cells Devoid of the γ-Polypeptide. We have recently shown that the EPR signals and redox characteristics of the iron–sulfur centers of the native nitrate reductase are not fundamentally changed when the enzyme lacks the membrane-bound γ-subunit and the reductase is, therefore, soluble and active only with benzyl viologen (Augier et al., in press). Accordingly, plasmid pVA7-(*narJ*) was used together with plasmid pVA50 derivatives carrying the wild *narG* allele and either the wild or a mutated *narH* allele. As expected from previous studies, the enzyme produced in these conditions by cells carrying wild alleles was located almost exclusively in the soluble fraction (96%), and its specific activity was identical to that of the membrane-bound enzyme (Tables III and IV). When the mutated *narH* alleles replaced the wild one, the same cellular location was observed; the specific activities, however, were lower than that of the control enzyme but, in each case, correlated very well with the activity measured when the γ-subunit was present (Tables III and IV).

The soluble mutant enzymes were purified as indicated in the Experimental Procedures and compared to the wild-type soluble enzyme. It is interesting to note that all three are eluted at the same NaCl concentration as the native or control enzymes. In addition, they have the same estimated relative molecular weight of about 200 000 (data not show), and their subunit composition is identical ($\alpha = 150\,000$ and $\beta = 60\,000$; Figure 1) to that of the native enzyme.

As shown by DeMoss et al. (1977), it is known that the β-subunit of the enzyme can be cleaved into a β′-form with relative molecular weight 43 000 by a trypsin treatment which does not affect the α-subunit. The same result was observed with the control and mutant enzymes, $\alpha\beta(C_{16}A)$, $\alpha\beta(C_{19}A)$, or $\alpha\beta(C_{19}S)$, partially purified from the soluble fraction of strains lacking the γ-subunit (Figure 1; data not shown for the $\alpha\beta(C_{19}A$ or S) mutant enzymes).

EPR Study of the Mutant Nitrate Reductases in Cells Devoid of the γ-Polypeptide. We have previously shown that the four iron–sulfur centers of nitrate reductase belong to two

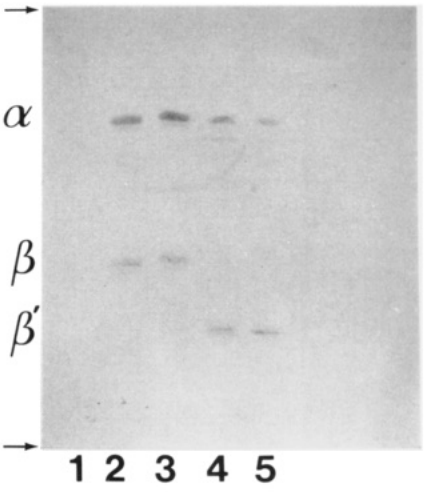

FIGURE 1: Analysis by immunoblotting of the subunit composition of various mutant nitrate reductases: effect of trypsin digestion. Trypsination, electrophoresis, and Western blotting of partially purified nitrate reductases were performed as described in the Experimental Procedures. Lane 1: 2 μg of Triton X-100-solubilized crude extract of strain LCB79. Lane 2: 1 μg of partially purified nitrate reductase of strain LCB79/pVA7+pVA50. Lane 3: 1 μg of partially purified nitrate reductase of strain LCB79/pVA7+pVA50C_{16}A. Lane 4: Sample as in lane 2, but trypsinated. Lane 5: Sample as in lane 3, but trypsinated. The arrows indicate the beginning and the end of the migration.

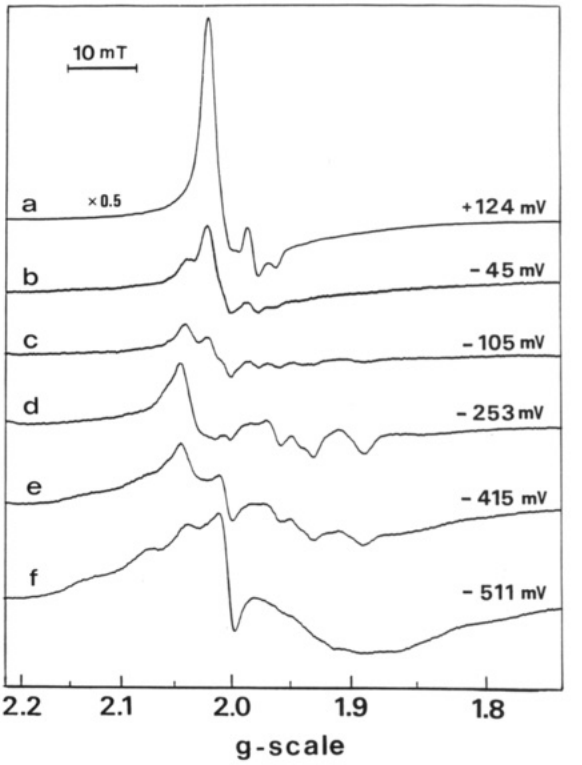

FIGURE 2: Representative EPR spectra obtained during the redox titration of $\alpha\beta(C_{16}A)$ nitrate reductase. Experimental conditions: temperature, 15 K; mirowave frequency, 9.305 GHz; microwave power, 100 mW; modulation frequency, 100 kHz; modulation amplitude, 0.5 mT.

groups whose redox potentials differ by more than 200 mV. Therefore, the study of the redox characteristics of the iron–sulfur centers in the mutant enzymes required the performance of redox titrations over a wide range of potentials, typically from +200 to −500 mV. Figures 2–4 show representative EPR spectra given by the $\alpha\beta(C_{16}A)$, $\alpha\beta(C_{19}S)$, and $\alpha\beta(C_{19}A)$ mutant proteins, respectively, poised at several characteristic redox potentials chosen in this range. The redox behavior of

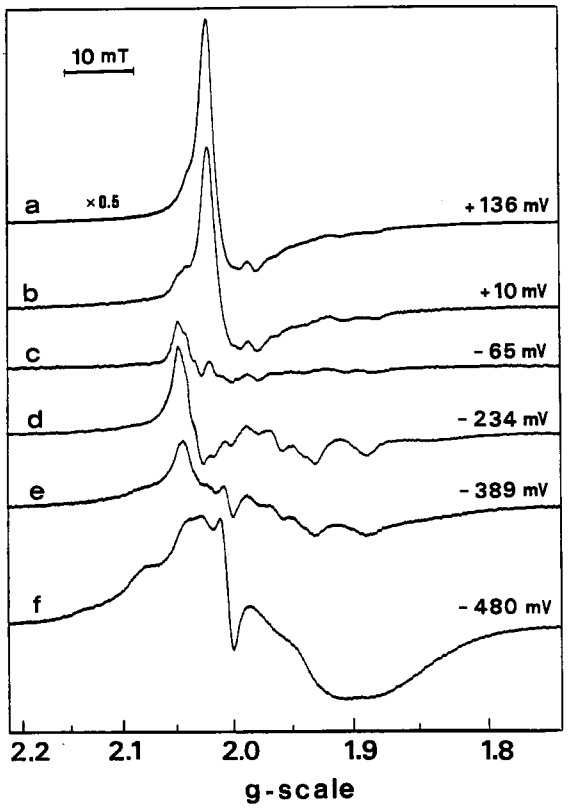

FIGURE 3: Representative EPR spectra obtained during the redox titration of the $\alpha\beta(C_{19}S)$ nitrate reductase. Experimental conditions were the same as in Figure 2.

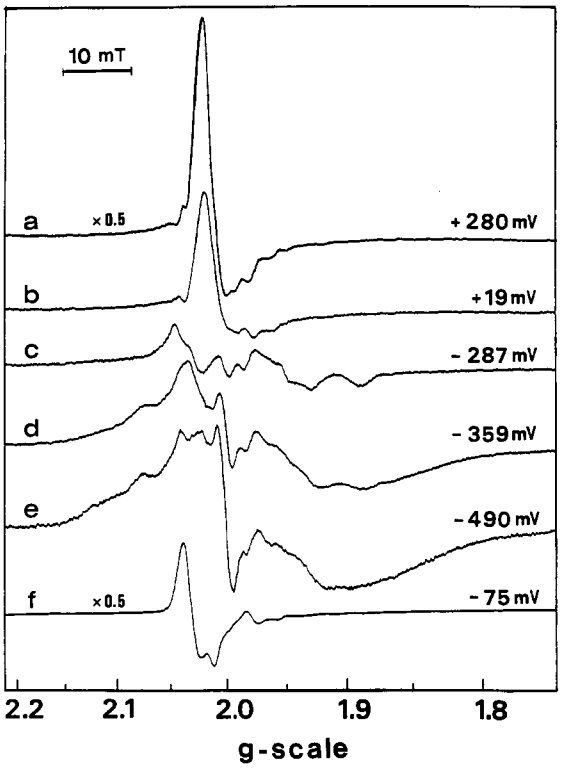

FIGURE 4: Representative EPR spectra obtained during the redox titration of the $\alpha\beta(C_{19}A)$ nitrate reductase. Experimental conditions were the same as in Figure 2. Spectra a–e result from the difference between the experimental spectra and spectrum f recorded at –75 mV. At this potential, the spectrum given by the $\alpha\beta(C_{19}A)$ mutant protein contains only the Fe–NO contribution.

the EPR spectra was very similar to the three mutant proteins and, for the most part, followed that observed for the native enzyme (Guigliarelli et al., 1992; Augier et al., in press).

In the oxidized state, the EPR spectrum consists of a typical $[3Fe–4S]^+$ signal, on which are superimposed minor features due to a partially saturated high-pH Mo^V signal (Figures 2a, 3a, and 4a). Upon reduction, these two signals progressively disappear while a slowly relaxing signal develops in the g = 2.04 region (Figures 2b, 3b, and 4b). In previous work, we showed that this signal was preparation dependent and was probably associated with adventitious iron–nitrosyl complexes (Augier et al., in press). In the case of the $\alpha\beta(C_{16}A)$ and $\alpha\beta(C_{19}S)$ mutant proteins, this Fe–NO signal reaches its maximum amplitude at about –100 mV, but gives only a minor contribution to the high microwave power EPR spectra (Figures 2c and 3c). However, in the case of the $\alpha\beta(C_{19}A)$ mutant protein, the Fe–NO signal is much more pronounced, but its amplitude does not depend on the redox potential. This signal (Figure 4f) has been subtracted from all experimental spectra to allow a detailed analysis of the $\alpha\beta(C_{19}A)$ iron–sulfur center signals (Figure 4).

For each mutant protein, the amplitude of the $[3Fe–4S]^+$ signal measured at g = 2.02 was plotted against the redox potential (Figures 5a, 6a, and 7a). The experimental data can be fit with Nernst curves whose midpoint potentials are equal to 0, +30, and +80 mV for the $\alpha\beta(C_{16}A)$, $\alpha\beta(C_{19}S)$, and $\alpha\beta(C_{19}A)$ mutant enzymes, respectively. The peak to peak amplitude of the Mo^V peak at g = 1.98 has also been measured on EPR spectra recorded with a lower microwave power (1 mW) to determine the midpoint potential of the MO^{IV}/Mo^V couple (not shown). The values +40 and +30 mV found for $\alpha\beta(C_{16}A)$ and $\alpha\beta(C_{19}S)$ mutant enzymes, respectively, are slightly less positive than that of the native enzyme (+80mV) (Guigliarelli et al., 1992). In the case of the $\alpha\beta(C_{19}A)$ mutant enzyme, the variation of the Mo^V signal showed a marked departure from a Nernst plot, so that no reliable midpoint potential could be determined. The same problem was encountered with some other mutants in a previous work (Augier et al., in press). It is important to note that the composite rhombic signal, given by center 1 in wild-type nitrate reductase in the range +100 to –100 mV, was not observed in any of the three mutants: at about –100 mV, where this signal was maximal in the native enzyme (Guigliarelli et al., 1992), only the Fe–NO signal could be detected (Figures 2c, 3c, and 4f).

For potentials more negative than –100 mV, a rhombic signal appears with peaks at g = 1.89, 1.93, and around 2.05 in a region where the main peak of the Fe–NO signal is overlapping (Figures 2d, 3d, and 4c). This signal is characterized by relatively broad wings on the high-field and low-field parts, and an additional sharp derivative-like feature is visible at g = 1.96 in the $\alpha\beta(C_{16}A)$ and $\alpha\beta(C_{19}S)$ mutant enzymes. At lower potentials, broad outer lines develop at g = 2.08 and 1.84, and the rhombic signal is progressively replaced by a broad, featureless spectrum typical of magnetically interacting $[4Fe–4S]^+$ centers (Figures 2–4). When the amplitudes of the EPR spectra measured at different g values are plotted as a function of the potential, two reduction steps are observed. This reveals the successive reduction of, at least, two [4Fe–4S] centers whose EPR signals are overlapping (Figures 5a, 6a, and 7a). For the $\alpha\beta(C_{16}A)$ and $\alpha\beta(C_{19}S)$ mutant enzymes, the redox titration of the g = 1.96 feature is well described by a single Nernst curve centered around –190 mV, while the amplitude variations at g = 2.08 show two waves centered at about –190 and –430 mV, with the lowest potential wave corresponding to the appearance of the interaction spectrum. In the case of the $\alpha\beta(C_{19}A)$ mutant enzyme, there is no derivative-like structure at g = 1.96, and

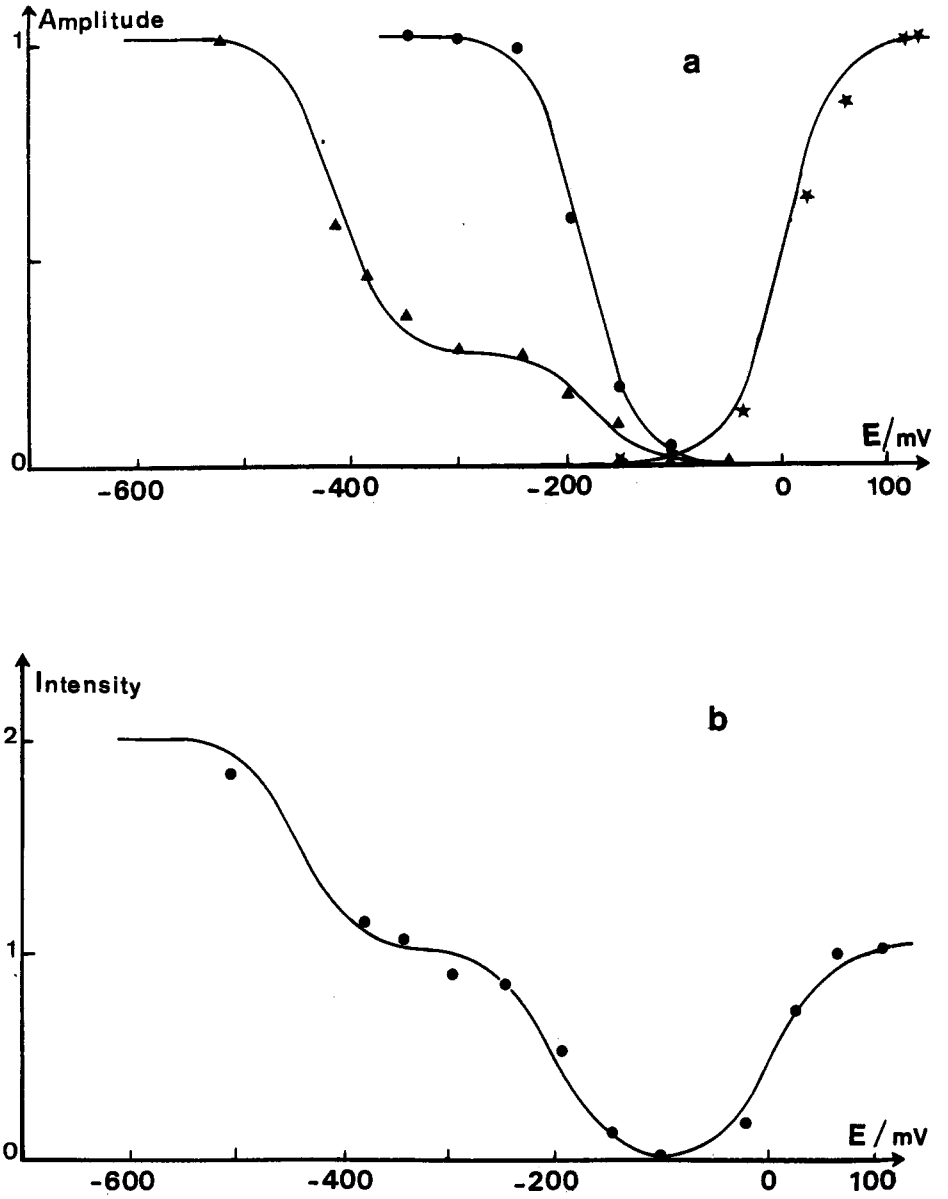

FIGURE 5: Redox behavior of the iron–sulfur center EPR signals in the $\alpha\beta(C_{16}A)$ nitrate reductase. (a) Normalized amplitude variations measured at $g = 2.02$ (★) for the $[3Fe–4S]^+$ signal and at $g = 1.96$ (●) and $g = 2.08$ (▲) for the $[4Fe–4S]^+$ signals. (b) Normalized intensity variations of the EPR spectra recorded with the same conditions as in Figure 2. Intensity measurements were corrected for power saturation effects and normalized as indicated in the text. The continuous lines represent Nernst plots centered at 0, −180, and −440 mV.

the measurements are carried out at $g = 1.89$ and 2.08. Two reduction waves are also observed, but the full development of the interaction spectrum occurs at a markedly higher potential (Figure 7a).

In order to determine the stoichiometry of the different iron–sulfur centers in the mutant enzymes, integrated intensity measurements of the EPR spectra were performed over the whole range of potentials. These measurements were done at high microwave power (100 mW) to minimize the Mo^V and Fe–NO spectral contributions. At 100 mW, the iron–sulfur EPR signals are partially saturated, and it was necessary to correct the experimental integrated intensity for saturation effects. This was done by comparing the amplitude measured at 100 mW with that measured under nonsaturating conditions (1 mW) for the different signals: (i) the $g = 2.02$ peak for the $[3Fe–4S]^+$ signal in oxidized samples; (ii) the $g = 1.89$ peak for the rhombic signal in samples poised at about −250 mV; and (iii) the amplitude at $g = 1.89$ for the interaction signal in fully reduced samples. At 15 K and 100 mW, power saturation effects were nearly the same for all mutant enzymes and typically induced a 10–20% decrease in the intensity for the $[3Fe–4S]^+$ and interaction signals, but a 60% decrease in the rhombic signal intensity. After correction for microwave power saturation, relative integrated intensities have been normalized by taking the $[3Fe–4S]^+$ signal intensity in the fully oxidized state as unity and have been plotted against the redox potential. The results clearly show that, for the three mutant enzymes, the iron–sulfur centers associated with each reduction step are in a 1:1:1 ratio (Figures 5b, 6b, and 7b). Moreover, the intensity variations are well fit by Nernst curves centered on the midpoint potentials deduced from the amplitude titrations (Figures 5a, 6a, and 7a). If we consider that the $[3Fe–4S]^+$ signal of the mutants corresponds to 1 spin per molecule, then the interaction signal represents 2 spins per molecule in the fully reduced state of these enzymes.

DISCUSSION

As pointed out in the introduction, the first or second Cys residue of group I was substituted by site-directed mutagenesis, leading to the $\beta(C_{16}A)$, $\beta(C_{19}A)$, and $\beta(C_{19}S)$ mutant proteins.

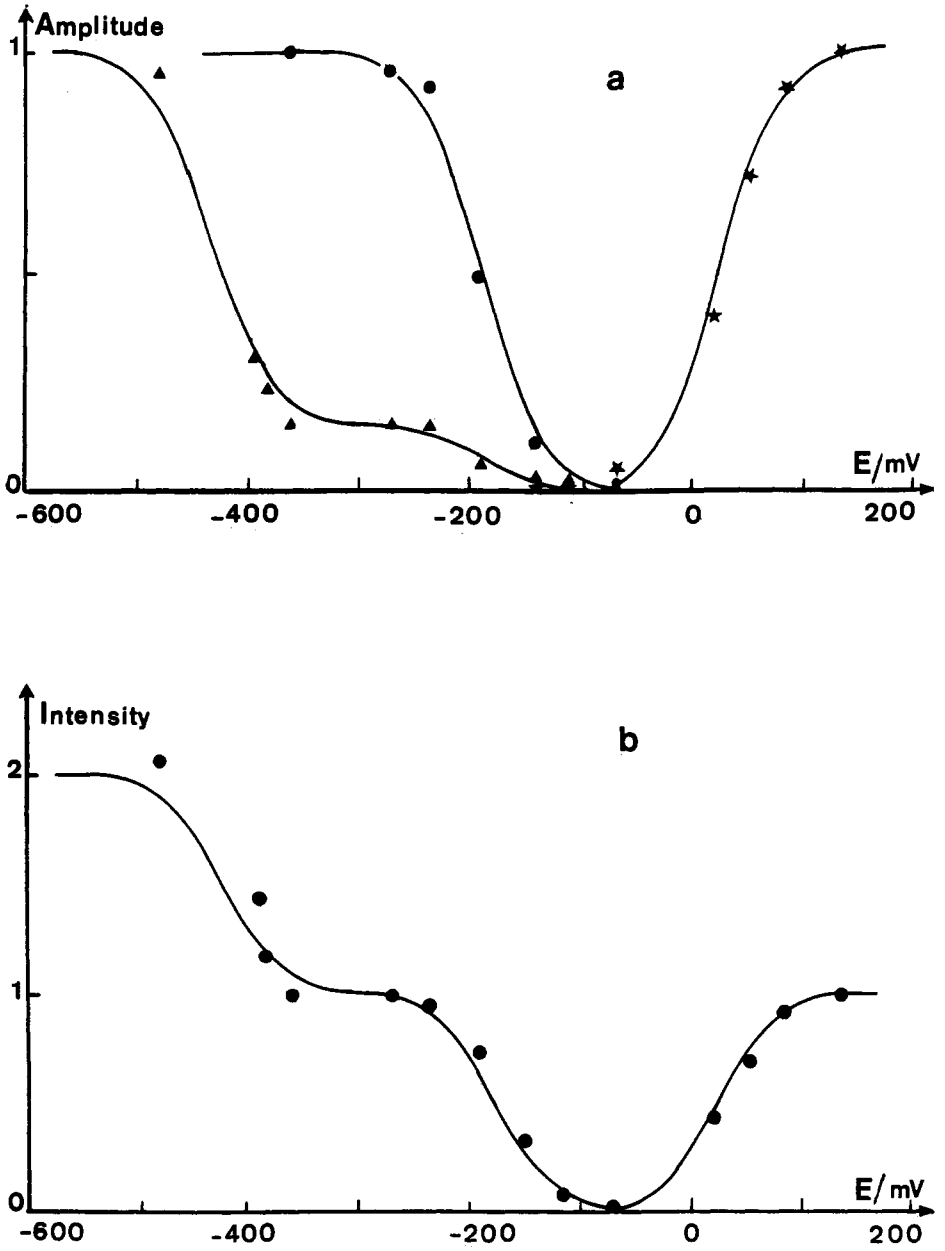

FIGURE 6: Redox behavior of the iron–sulfur center EPR signals in the $\alpha\beta(C_{19}S)$ nitrate reductase. (a) Normalized amplitude variations measured at $g = 2.02$ (★) for the $[3Fe–4S]^+$ signal and at $g = 1.96$ (●) and $g = 2.08$ (▲) for the $[4Fe–4S]^+$ signals. (b) Normalized intensity variations of the EPR spectra recorded with the same conditions as in Figure 2. Intensity measurements were corrected for power saturation effects and normalized as indicated in the text. The continuous lines represent Nernst plots centered at +30, −190, and −430 mV.

With small variations, equivalent results were observed for the three mutant proteins. The mutant enzymes were found to be as abundant and as stably bound to the membrane as the native enzyme was when the γ-subunit was present. In addition, the $\alpha\beta^*$ purified mutant complexes did not show any differences in terms of trypsin proteolysis from the native $\alpha\beta$ complex, and they contained the molybdenum cofactor. However, when assayed with their physiological electron donor, these mutant enzymes displayed only one-third of the activity of the native enzyme.

Studies on the variations of EPR intensity as a function of redox potential indicated that these enzymes only contain three iron–sulfur centers instead of the four present in the native enzyme. In the oxidized state, the mutant enzymes gave a $[3Fe–4S]^+$ signal identical to that given by the native enzyme. Moreover, the redox potential of this [3Fe–4S] center remains close to that of center 2 of the wild-type enzyme (Table V). When the redox potential was lowered to values where the rhombic signal of the [4Fe–4S] center of the native enzyme (center 1) should appear, no such signal was detected in the mutant enzymes. Lowering the redox potential further resulted in the appearance of signals corresponding to two [4Fe–4S] centers with very low redox potentials. These observations could be explained by assuming that, in the mutant enzymes, the redox potential decreased by about 300 mV for center 1, 200 mV for center 3, and 100 mV for center 4, leading this last center to be reduced incompletely at −500 mV. Such an interpretation seems to be very unlikely because it should imply that each point mutation induces concomitant and considerable shifts of the three [4Fe–4S] centers' redox potentials. In fact, one of these two centers presented characteristics similar to those of center 3 of the native enzyme: a redox potential around −200 mV, a broad EPR signal, and a slower spin-lattice relaxation than the other centers. In addition, the other center was probably identical to center 4 in the native enzyme since its redox potential was about −400 mV and its reduction also gave an EPR spectrum showing magnetic interactions with other [4Fe–4S] centers.

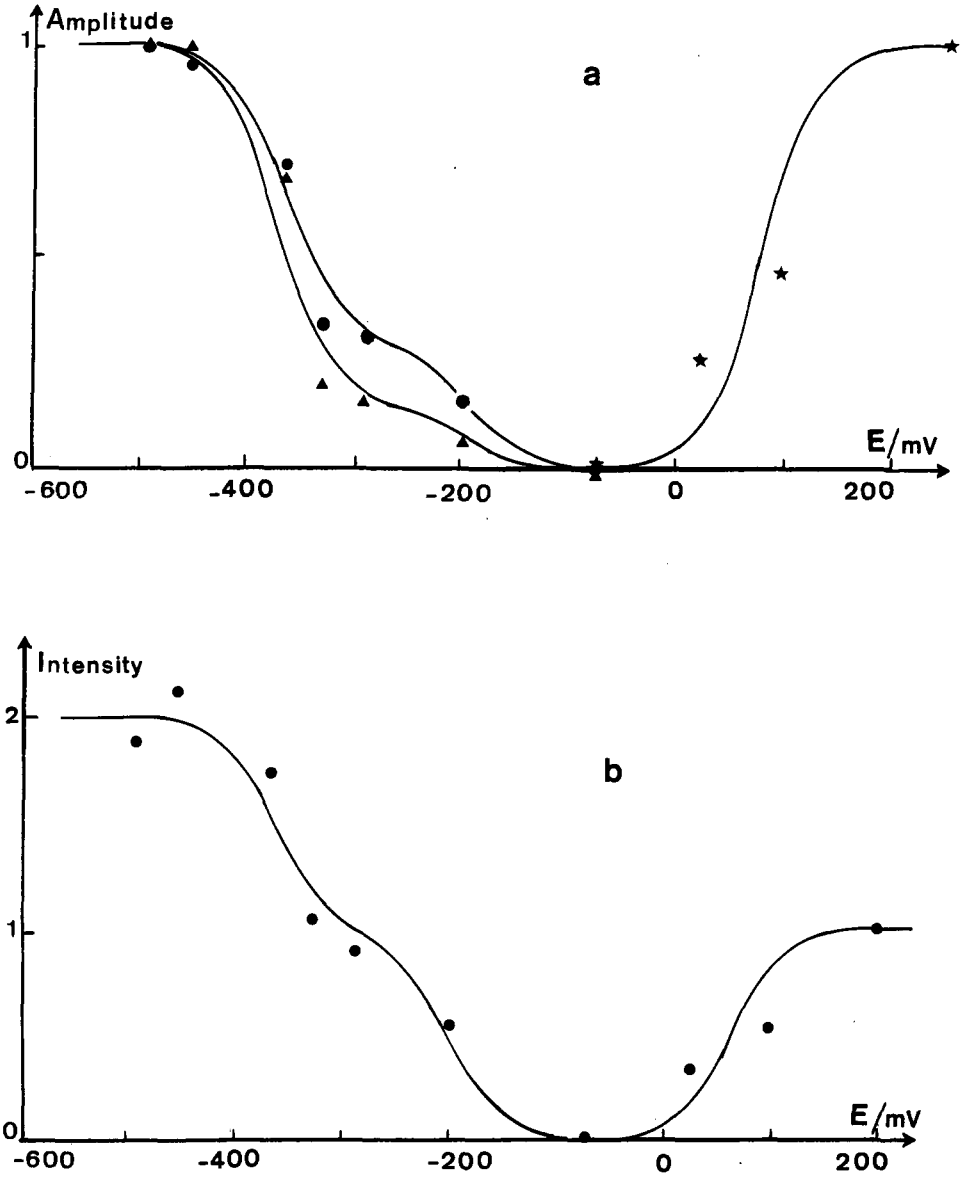

FIGURE 7: Redox behavior of the iron–sulfur center EPR signals in the $\alpha\beta(C_{19}A)$ nitrate reductase. Amplitude and intensity measurements were performed after subtraction of the Fe–NO signal contribution (see Figure 4). (a) Normalized amplitude variations measured at g = 2.02 (★) for the $[3Fe–4S]^+$ signal and at g = 1.89 (●) and g = 2.08 (▲) for the $[4Fe–4S]^+$ signals. (b) Normalized intensity variations of the EPR spectra obtained with the same conditions as in Figure 4. Intensity measurements were corrected for power saturation effects and normalized as indicated in the text. The continuous lines represent Nernst plots centered at +80, −190, and −370 mV.

Therefore, we can conclude that the substitutions at positions Cys_{16} or Cys_{19} of the β-subunit of the enzyme led to the disappearance of center 1, indicating that the first two—and probably also the third—Cys residues of group I are ligands of center 1, the highest potential [4Fe–4S] center in the native enzyme. The loss of center 1 did not affect either the stable integration of centers 2–4 in the mutant enzymes or their EPR and redox characteristics, indicating that the folding around these centers was only slightly modified. Furthermore, the two-thirds decrease in nitrate reductase activity in the mutant enzymes lacking center 1 strongly suggests that this center is involved in intramolecular electron transfer within the native enzyme.

The role of the low-potential centers 3 and 4 in nitrate reductase remains elusive. Theoretically, the values of their redox potentials (below −200 mV) would exclude these centers from the electron pathway between quinones (−80 mV) and nitrate (+420 mV). Nevertheless, as already discussed for the low-potential centers of fumarate reductase (Manodori et al., 1992), one could suppose that the midpoint potential of these centers, as determined by equilibrium redox titration, was much lower than their intrinsic potential, due to strong anti-cooperative redox interactions with centers of much higher redox potential. If such were the case for the nitrate reductase enzyme, one would expect the midpoint potential of centers 3 and 4 to suffer drastic changes when center 1 is lost. No such changes have been observed in any of the mutant enzymes lacking this center, making this possibility unlikely. More likely, as previously suggested by Augier et al. (in press), it seems that these centers have essentially a structural role in the stabilization of the three-dimensional structure of the $\alpha\beta$ complex. Note that such a structural role has recently been proposed for center 2 of fumarate reductase (Manodori et al., 1992) and for the [4Fe–4S] center of endonuclease III of *E. coli* (Fu et al., 1992).

The significant nitrate reductase activity of the $\alpha\beta(C_{16}A)$, $\alpha\beta(C_{19}A)$, and $\alpha\beta(C_{19}S)$ mutant enzymes shows that center 1 is not indispensable for enzymatic activity. If, as suggested above, centers 3 and 4 do not participate in electron transfer, then our results show that nitrate reductase can function with

Table V: Midpoint Potentials of the Iron–Sulfur Centers in the Wild-Type and Mutant Nitrate Reductases from *E. coli*

strain	midpoint potentials[a] (mV) center 1 [4Fe–4S]	center 2 [3Fe–4S]	center 3 [4Fe–4S]	center 4 [4Fe–4S]	references
MC4100	+60	+20	–200	–400	Guigliarelli et al. (1992)
	(+80)[b]	(+60)[b]			Augier et al. (in press)
LCB79/ pVA7+ pVA50	+90	+20	ND	ND	Augier et al. (in press)
LCB79/ pVA7+ pVA50C_{16}A		0	–180	–440	this work
LCB79/ pVA7+ pVA50C_{19}A		+80	–190	–370	this work
LCB79/ pVA7+ pVA50C_{19}S		+30	–190	–430	this work

[a] These midpoint potentials are those of the Nernstian curves which gave the best fit of the experimental data. [b] The high quality of the experimental data obtained with the native enzyme allowed us to show that centers 1 and 2 are likely coupled by an anti-cooperative redox interaction. These values correspond to the microscopic redox potentials deduced from this analysis (Guigliarelli et al., 1992). ND: not determined.

its single [3Fe–4S] center (center 2) to transfer electrons from the redox centers of the γ-subunit to the molybdenum cofactor of the α-subunit. The same function has recently been proposed for the [3Fe–4S] center in fumarate reductase of *E. coli* (Manodori et al., 1992). In this context, both high-potential centers, centers 1 and 2 of nitrate reductase, would participate independently and in parallel in electron transfer to the molybdenum cofactor. This could be taken as an indication that both centers are in the vicinity of the molybdenum cofactor even if they are not close to one another, as suggested by the apparent unchanged characteristics of center 2 when center 1 is missing.

Taking into account all of our results, we can now assign groups of Cys residues (I–IV) to particular iron–sulfur centers in the β-subunit of nitrate reductase. On the basis of an analysis of the αβ(C_{184}S) mutant enzyme, we previously proposed that the first three Cys residues of group II (Cys_{184}, Cys_{187}, and Cys_{192}) were ligands of center 3 (Augier et al., in press). Center 2 was tentatively attributed to group III on the following basis: all known [3Fe–4S] centers are coordinated by ferredoxin-like groups of Cys residues in which the second cysteine residue is missing or is not used for iron coordination. This position (aa220) is not occupied by a cysteinyl residue but by a tryptophanyl residue in the β-subunit of nitrate reductase, and we have shown that this position can be substituted by various residues without losing the [3Fe–4S] center and without strongly affecting physiological electron transfer to any great extent (Augier et al., in press). In the present work, we have demonstrated that the first two Cys residues of group I and probably also the third are ligands of center 1 of native nitrate reductase. According to the above arguments, the only possible assignment for the first three Cys residues of group IV is that they must be involved in forming center 4, as indicated in Figure 8.

DMSO reductase is a molybdoenzyme closely related to nitrate reductase, and its DmsB subunit is very similar to the NarH subunit. DmsB contains four groups of four Cys residues and carries four [4Fe–4S] centers (Cammack & Weiner, 1990). The substitution of Cys_{102} by Trp, Ser, Tyr, or Phe in this subunit led to the transformation of a [4Fe–4S] center into a [3Fe–4S] center (Rothery & Weiner, 1991). Taking into account the strong similarity between the NarH and DmsB subunits, we are tempted to extend tentatively the model proposed for NarH to DmsB. On the basis of EPR data, we have previously established a correspondence between (i) center 1 of DmsB and center 1 of NarH and (ii) center 2 of DmsB and center 2 of NarH. We propose that, in DmsB, center 1 (–50 mV) is bound to Cys_{14}, Cys_{17}, and Cys_{20} of Cys group I and center 2 (–120 mV) is bound to Cys_{99}, Cys_{102}, and Cys_{105} or Cys group III. The low-potential [4Fe–4S] centers would then be assigned to Cys groups II and IV in DmsD, but no experimental data are currently available to complete this assignment.

Apart from the unambiguous link between center 1 and Cys group I, all other partnerships between a center and a Cys arrangement could be confirmed by further experiments. In particular, it would be of interest to perform a more detailed EPR study of the β(C_{184}S) mutant protein, as well as of mutant proteins in which the environment of residue 220 (see above) would be changed in such a way that the EPR and redox characteristics of the center coordinated by the Cys_{217} and Cys_{223} residues would be changed.

The data presented here are in total contrast to those we have reported for each of the other three centers, the loss of which was detrimental to the integration of all centers and of the molybdenum cofactor. It is therefore clear that, in terms of integration and/or stabilization of iron–sulfur centers and of molybdenum cofactor in the native enzyme, center 1 does not play the same role as that played by any other center, since the mutant enzymes lacking this center contain the iron–sulfur centers 2–4 and molybdenum. There is no evidence in the literature to prove whether iron–sulfur centers are assembled simultaneously or sequentially. However, from all our results, we can speculate that the assembly could begin with the interdependent and stable integration of centers 2–4. This would yield an intermediate structure—resembling that found in the mutated αβ(C_{16}A), αβ(C_{19}A), or αβ(C_{19}S) subunit—in which these centers would almost be in the same relative conformation as in the final native enzyme. Whether this integration occurs in a free β*-subunit or in a β*-subunit already bound to the α-subunit could be tested in a cell expressing the β*-subunit alone: β(C_{16}A), for example. That the first possibility could well be the case is indirectly supported

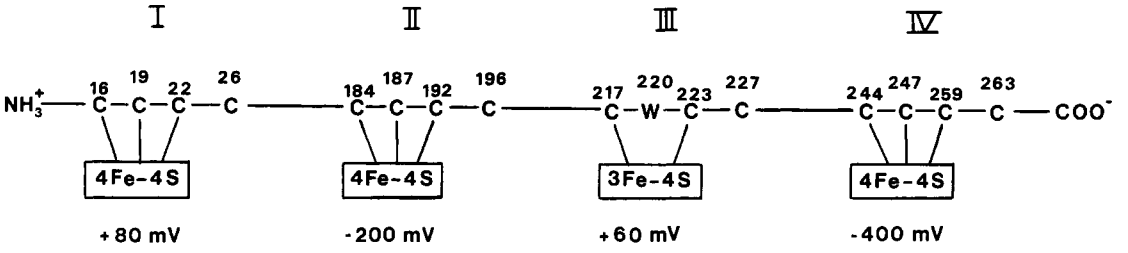

FIGURE 8: Proposed model for the coordination of the four iron–sulfur centers to the four cysteine groups (I–IV) of the β-subunit from nitrate reductase. The midpoint potential for each iron–sulfur center is indicated.

by the work of Johnson et al. (1988) on the fumarate reductase enzyme. This respiratory system is related to nitrate reductase in that the FrdB subunit is an electron-transfer unit with three iron–sulfur centers coordinated by ferredoxin-like Cys arrangements. These authors have demonstrated that the FrdB subunit produced alone in vivo from a plasmid is able to coordinate two out of the three iron–sulfur centers of the native complex. In our case, whether the structure in which iron–sulfur centers is integrated, β alone, or $\alpha\beta$ complex, one can suppose that once centers 2–4 are present, center 1 can then be integrated into β and the molybdenum cofactor into α.

CONCLUSION

The main finding of this work is that the [4Fe–4S] of high redox potential (center 1, +80 mV) can be lost without affecting the stable integration of the other centers or the stability of the final $\alpha\beta^*$ complex. To our knowledge, this is the first report that, upon a single cysteinyl residue substitution, a multi-iron–sulfur center protein can lose only one center and still form a physiologically active complex. Related data have been published concerning the FrdB subunit (Johnson et al., 1988). In this case the FrdB subunit was deleted from its C-terminal and as far as the third Cys group. This led to a truncated subunit lacking the [3Fe–4S] center and possessing only the other two iron–sulfur centers, the [2Fe–2S] and [4Fe–4S] centers. It must be pointed out, however, that no attempt was made to determine whether this truncated subunit could bind to the FrdA subunit and constitute an active complex.

Usually, the first Cys residues of a ferredoxin-like Cys arrangement are ligands for iron atoms belonging to one center, while the last Cys residue is involved in the coordination of an iron atom of another center. Thus, the Cys residues of one arrangement participate in liganding two different centers, while one center is linked to two different Cys groups. Since three iron atoms of center 1 are bound by three Cys residues of group I, it would be of interest to identify the Cys residue which binds the fourth iron atom of this center. There are five putative candidates: three of them are the fourth Cys residues of groups II–IV. The other candidates are the two Cys residues of β which do not belong to any Cys group. Experiments are in progress to resolve this.

ACKNOWLEDGMENT

We thank Dr. Gordon Barr for a critical reading of the manuscript.

REFERENCES

Augier, V., Guigliarelli, B., Asso, M., Bertrand, P., Frixon, C., Giordano, G., Chippaux, M., & Blasco, F. (1993) *Biochemistry* (in press).

Blasco, F., Iobbi, C., Giordano, G., Chippaux, M., & Bonnefoy, V. (1989) *Mol. Gen. Genet. 218*, 249–256.

Blasco, F., Nunzi, F., Pommier, J., Brasseur, R., Chippaux, M., & Giordano, G. (1992) *Mol. Microbiol. 6*, 209–219.

Cammack, R., & Weiner, J. H. (1990) *Biochemistry 29*, 8410–8416.

DeMoss, J. A. (1977) *J. Biol. Chem. 252*, 1696–1701.

Fu, W., O'Handley, S., Cunningham, R. P., & Johnson, M. K. (1992) *J. Biol. Chem. 267*, 16135–16137.

Giordano, G., Grillet, L., Rosset, R., Dou, J. H., Azoulay, E., & Haddock, B. A. (1978) *Biochem. J. 176*, 553–561.

Graham, A., & Boxer, D. H. (1980) *Biochem. Soc. Trans. 8*, 329–330.

Graham, A., Jenkins, H. E., Smith, N. H., Mandrand-Berthelot, M. A., Haddock, B. A., & Boxer, D. H. (1980) *FEMS Microbiol. Lett. 7*, 145–151.

Guigliarelli, B., Asso, M., More, C., Augier, V., Blasco, F., Pommier, J., Giordano, G., & Bertrand, P. (1992) *Eur. J. Biochem. 207*, 61–68.

Iobbi, C., Santini, C. L., Bonnefoy, V., & Giordano, G. (1987) *Eur. J. Biochem. 168*, 451–459.

Johnson, J. L., Hainline, B. E., Rajagopalan, K. V., & Arison, B. H. (1984) *J. Biol. Chem. 259*, 5414–5422.

Johnson, M. K., Bennett, D. E., Morningstar, J. E., Adams, M. W., & Mortenson, L. E. (1985) *J. Biol. Chem. 260*, 5456–5463.

Johnson, M. K., Kowal, A. T., Morningstar, J. E., Oliver, M. E., Whittaker, Gunsalus, R. P., Ackrell, B. A. C., & Cecchini, G. (1988) *J. Biol. Chem. 263*, 14732–14738.

Jones, R. W., & Garland, P. B. (1977) *Biochem. J. 164*, 199–211.

Kent, H. M., Ionnidis, I., Gormal, C., Smith, B. E., & Buck, M. (1989) *Biochem. J. 264*, 257–264.

Laemmli, U. K. (1970) *Nature 227*, 680–685.

Lowry, O. L., Rosenbrough, N. J., Farr, A. L., & Randall, R. J. (1951) *J. Biol. Chem. 193*, 265–275.

MacGregor, C. H. (1975) *J. Bacteriol. 121*, 1111–1116.

Maniatis, T., Frisch, E. F., & Sambrook, J. (1982) *Molecular cloning: a laboratory manual*, Cold Spring Harbor Laboratory, Cold Spring Harbor, NY.

Manodori, A., Cecchini, G., Schröder, I., Gunsalus, R. P., Werth, M. T., & Johnson, M. K. (1992) *Biochemistry 31*, 2703–2712.

May, H. D., Dean, D. R., & Newton, W. E. (1991) *Biochem. J. 277*, 457–464.

Pichinoty, F. (1969) *Arch. Microbiol. 68*, 51–64.

Rothery, R. A., & Weiner, J. H. (1991) *Biochemistry 30*, 8296–8305.

Saracino, L., Violet, M., Boxer, D., & Giordano, G. (1986) *Eur. J. Biochem. 158*, 483–490.

Sodergren, E. J., & DeMoss, J. A. (1988) *J. Bacteriol. 170*, 1721–1729.

Taylor, J. W., Ott, J., & Eckstein, F. (1985) *Nucleic Acids Res. 13*, 8764–8785.

Towbin, H., Stachelin, T. L., & Gordon, J. (1979) *Proc. Natl. Acad. Sci. U.S.A. 76*, 4350–4356.

Werth, M. T., Cecchini, G., Manodori, A., Ackrell, B. A. C., Schröder, I., Gunsalus, R. P., & Johnson, M. K. (1990) *Proc. Natl. Acad. Sci. U.S.A. 87*, 8965–8969.